

1 **Quantitative Holocene climatic reconstructions for the lower Yangtze region**
2 **of China**

3 **Jianyong Li** ^{1, *} • **John Dodson** ^{1, 2, *} • **Hong Yan** ^{1, *} • **Weiming Wang** ^{3, *} • **James B. Innes** ^{4,}
4 ***** • **Yongqiang Zong** ^{5, 6} • **Xiaojian Zhang** ⁷ • **Qinghai Xu** ⁸ • **Jian Ni** ⁹ • **Fengyan Lu** ¹

5 ¹ State Key Laboratory of Loess and Quaternary Geology, Institute of Earth Environment, Chinese
6 Academy of Sciences, Xi'an 710075, China. ² School of Biological, Earth and Environmental Sciences,
7 University of New South Wales, Sydney 2033, Australia. ³ Key Laboratory of Economic Stratigraphy
8 and Palaeogeography, Nanjing Institute of Geology and Palaeontology, Chinese Academy of Sciences,
9 Nanjing 210008, China. ⁴ Geography Department, Durham University, Durham DH1 3LE, UK. ⁵
10 Department of Earth Sciences, The University of Hong Kong, Hong Kong Special Administrative
11 Region, China. ⁶ Guangzhou Institute of Geography, Guangzhou 510070, China. ⁷ School of
12 Geographic and Oceanographic Sciences, Nanjing University, Nanjing 210093, China. ⁸ Institute of
13 Nihewan Archaeology, Hebei Normal University, Shijiazhuang 050024, China. ⁹ College of Chemistry
14 and Life Sciences, Zhejiang Normal University, Jinhua 321004, China.

15

16 *Correspondence authors: **Jianyong Li** (lijy@ieecas.cn), **John Dodson** (john@ieecas.cn), **Hong Yan**
17 (yanhong@ieecas.cn), **Weiming Wang** (wmwang@nigpas.ac.cn), and **James B. Innes**
18 (j.b.innes@durham.ac.uk).

19

20 Address: State Key Laboratory of Loess and Quaternary Geology, Institute of Earth Environment,
21 Chinese Academy of Sciences, Xi'an 710075, China, telephone number: +86-029-62336270; Key
22 Laboratory of Economic Stratigraphy and Palaeogeography, Nanjing Institute of Geology and
23 Palaeontology, Chinese Academy of Sciences, Nanjing 210008, China; Geography Department,
24 Durham University, Durham DH1 3LE, UK.

25 **Abstract**

26 Quantitative proxy-based and high-resolution palaeoclimatic datasets are scarce for the lower reaches
27 of the Yangtze River (LYR) basin. This region is in a transitional vegetation zone which is
28 climatologically sensitive; and as a birthplace for prehistorical civilization in China, it is important to
29 understand how palaeoclimatic dynamics played a role in affecting cultural development in the region.
30 We present a pollen-based and regionally-averaged Holocene climatic twin-dataset for mean total
31 annual precipitation (PANN) and mean annual temperature (TANN) covering the last 10,000 years for
32 the LYR region. This is based on the technique of weighted averaging-partial least squares regression
33 to establish robust calibration models for obtaining reliable climatic inferences. The pollen-based
34 reconstructions generally show an early Holocene climatic optimum with both abundant monsoonal
35 rainfall and warm thermal conditions, and a declining pattern of both PANN and TANN values in the
36 middle to late Holocene. The main driving forces behind the Holocene climatic changes in the LYR
37 area are likely summer solar insolation associated with tropical or subtropical macro-scale climatic
38 circulations such as the Intertropical Convergence Zone (ITCZ), Western Pacific Subtropical High
39 (WPSH), and El Niño/Southern Oscillation (ENSO). Regional multi-proxy comparisons indicate that
40 the Holocene variations in precipitation and temperature for the LYR region display an in-phase
41 relationship with other related proxy records from southern monsoonal China and the Indian monsoon-
42 influenced regions, but are inconsistent with the Holocene moisture or temperature records from
43 northern monsoonal China and the westerly-dominated region in northwestern China. Overall, our
44 comprehensive palaeoclimatic dataset and models may be significant tools for understanding the
45 Holocene Asian monsoonal evolution and for anticipating its future dynamics in eastern Asia.

46

47 **Keywords:** lower Yangtze, China, Holocene, climate, pollen, quantitative reconstructions

48

49

50

51 **1 Introduction**

52 The Yangtze River and its catchment occupy one of the largest drainage-basin systems in eastern Asian
53 continent and act as a boundary zone of northern and southern China (e.g. Zhao and Chen 1999; Wu
54 et al. 2012). The lower reaches of the Yangtze River (LYR) are situated in an area that is dominated by
55 the East Asian monsoonal circulation (EAM); and the natural vegetation is warm temperate broadleaf
56 and subtropical evergreen forests as well as transitions of these biomes (e.g. Ren and Beug 2002; Innes
57 et al. 2014). The vegetation and environment in the LYR region would have been sensitive to even
58 small-scale Holocene climatic as well as sea level fluctuations, due largely to its special bioclimatic
59 locality and any marked weakening or strengthening of the EAM regime (e.g. Morrill et al. 2003; Yi
60 et al. 2003; Zong et al. 2011). In particular, the LYR has been identified as one of the birthplaces for
61 prehistorical Chinese civilization such as the ancient Hemudu and Liangzhu Cultures, and for rice
62 cultivation such as the domesticated paddy *Oryza sativa*, as broadly elucidated by detailed
63 palaeoecological and archaeological evidence obtained in earlier studies (e.g. Londo et al. 2006; Zong
64 et al. 2007; Atahan et al. 2008; Fuller et al. 2009; Zhao et al. 2009; Li et al. 2010). As a consequence,
65 the LYR has thus been suggested as an ideal region of interest for exploring the history of Holocene
66 environmental, climatic, and cultural changes in eastern monsoonal China (e.g. Chen et al. 2005, 2009;
67 Innes et al. 2009, 2014; Wang et al. 2011, 2012; Zong et al. 2007, 2011, 2012).

68 Quantitatively-integrated and high-resolution records of Holocene precipitation and temperature
69 variations are rarely available in the LYR region, and the nature of Holocene climatic evolution in this
70 region remains unclear (e.g. An et al. 2000; Yi et al. 2003; Chen et al. 2005; Zong et al. 2006; Atahan
71 et al. 2008; Innes et al. 2009; Shu et al. 2010; Zong et al. 2011, 2012). Several questions arise, including
72 (i) has the Holocene climate evolved similarly or differently between the LYR and other EAM-affected
73 regions of China such as northern monsoonal China? (ii) What potential driving factors have possibly
74 triggered the Holocene climatic oscillations in the LYR? (iii) Have precipitation and temperature
75 patterns behaved synchronously or asynchronously during the course of Holocene in the LYR? (iv)
76 What was the timing and magnitude of the Holocene climatic optimum in the LYR? Making progress
77 on these issues requires regional-scale, high-resolution, and numerical palaeoclimatic data.

78 Quantitative palaeoclimatological estimates using biological fossil proxies preserved in sediments
79 provide an important avenue to develop these climatic data for comparison with regionally-averaged

80 and temporally-detailed Holocene precipitation as well as temperature data in northern China (e.g. Xu
81 et al. 2010; Chen et al. 2015; Li et al. 2015, 2017), the Tibetan Plateau (e.g. Shen et al. 2008; Herzschuh
82 et al. 2009; Wang et al. 2014), and many regions of Europe and North America (e.g. Seppä et al. 2009;
83 Bartlein et al. 2011; Vialou et al. 2012; Heiri et al. 2014; Mauri et al. 2015; Ladd et al. 2015), at local,
84 regional, and continental scales. The continuous and conceptual advances in developing and improving
85 large-scale calibration datasets and novel statistical techniques, have greatly promoted the accuracy
86 and robustness of climatic reconstructions, with different means of transforming a variety of fossil
87 biological assemblages into numerical estimates of past rainfall and temperature during the Holocene
88 (e.g. Birks et al. 2010; Salonen et al. 2014; Wang et al. 2014; Li et al. 2015, 2017). Such reconstructed
89 climatic data are particularly valuable for validating climatic transient-model simulations and other
90 independent climatic proxies comprising various geophysical, geochemical, and geocological records
91 from both terrestrial and marine environments worldwide (e.g. Braconnot et al. 2012; Renssen et al.
92 2012; Heiri et al. 2014; Li et al. 2015, 2017). In this respect, pollen data are one of the most commonly-
93 used biological proxies for quantitative Holocene terrestrial climatic inferences at a broad scale (e.g.
94 Seppä et al. 2009; Birks et al. 2010; Wang et al. 2014; Li et al. 2017).

95 In view of the above, we place a key focus on reporting new, high-resolution Holocene precipitation
96 and temperature reconstructions based on three fossil pollen sequences located within the lower
97 Yangtze region of monsoonal China. Our main purpose is to enable a broader understanding and
98 discussion with respect to the Holocene climate-related issues presented above regarding the LYR and
99 monsoonal China. We further assess our pollen-based Holocene climatic reconstructions by relying
100 upon an extensive multi-proxy comparison with a large number of either single or integrated moisture-
101 and temperature-related proxy records from China as well as other regions of the world, such as
102 speleothem oxygen isotope records (e.g. Fleitmann et al. 2003; Wang et al. 2005), loess-palaeosol
103 sequences (e.g. Wang et al. 2014; Li et al. 2014), lake sediment cores (e.g. Shen et al. 2005; Chen et
104 al. 2015), and climate model simulations (e.g. Jin et al. 2013; Chen et al. 2014). Moreover, the most
105 important element of this study is to contribute improved and meaningful insights for evaluating the
106 role of causal forces and atmospheric circulations in driving Holocene climatic, environmental, and
107 cultural changes as well as on forecasting their future possible dynamics in the lower Yangtze region

108 of China.

109 **2 Study area**

110 The lower valley of the Yangtze basin is located in the eastern part of monsoonal China (Fig. 1), where
111 the Asian monsoon dominates the climate and is characterized by warm, wet monsoon in summertime
112 and cold, dry monsoon in wintertime, with four well-pronounced climatic seasons occurring per year.
113 The 700 hPa atmospheric airstream lines in Figure 1 clearly show that the lower Yangtze region is
114 under the typical influence of the East Asian summer monsoon system, whilst northwestern and
115 southwestern China are dominated by the westerlies and Indian summer monsoon circulation,
116 respectively. Mean annual temperature (TANN) varies between 14.5 and 16.2 °C, and mean total
117 annual precipitation (PANN) ranges from 800 to 1400 mm, with its maximum level taking place in
118 July (e.g. Yi et al. 2006; Li et al. 2012). The area of our investigation is naturally covered by a high-
119 density of water-bodies including lakes, peats, bogs, marshes, swamps and wetlands, and it has thus
120 been particularly attractive for palaeoenvironmental studies (e.g. Tao et al. 2006; Innes et al. 2009,
121 2014; Wang et al. 2011, 2012). The vegetation of the LYR area is a biogeographical ecotone consisting
122 of mixed broad leaved deciduous and evergreen forests with distinct transitional characteristics (e.g.
123 Wu 1983; Huang and Zhang 2000). The main temperate components comprise species of *Betula*,
124 *Ulmus*, *Alnus*, *Populus*, *Quercus*, and *Acer*. The dominant evergreen components include *Castanopsis*,
125 *Cyclobalanopsis*, *Lithocarpus*, and Fagaceae. In addition, a low number of coniferous plant taxa such
126 as *Pinus*, *Picea*, and Cupressaceae occur in the high-elevation mountainous areas (e.g. Zong et al. 2011,
127 2012). It is therefore likely that in the transitional vegetation belt of the LYR, the Holocene climatic
128 variability would have caused a northward or southward shift of the temperate or subtropical biome
129 because of fluctuations in precipitation as well as temperature controlled primarily by the overall
130 variability of Eastern Asian summer monsoonal (EASM) intensity (e.g. Yi et al. 2006; Zong et al. 2007,
131 2011).

132 **3 Materials and methods**

133 Pollen-based quantitative estimates for both PANN and TANN were prepared from three Holocene
134 pollen datasets at Chaohu (Chen et al. 2009), Gucheng (Yang et al. 1996), and Pingwang (Innes et al.

135 2014), that lie within the lower reaches of the Yangtze catchment (Fig. 1). These fossil pollen profiles
136 were selected as they have reliable chronological control and fine-scale temporal resolution (see Table
137 1 for other details). The AMS radiocarbon technique was utilized to create geochronological datasets
138 (Yang et al. 1996; Chen et al. 2009; Innes et al. 2014). Plant macrofossils, shell fragments, pollen
139 residues, charcoal particles, and basal peats have been used for AMS dating (Yang et al. 1996; Chen
140 et al. 2009; Innes et al. 2014). The age–depth models were estimated by a linear interpolation between
141 adjacent samples (Yang et al. 1996; Chen et al. 2009; Innes et al. 2014). The radiocarbon dates were
142 calibrated and transformed to calendar years before present according to the IntCal13 calibration
143 dataset (Reimer et al. 2013). The AMS ^{14}C dates are presented here as cal. yr BP throughout the text.
144 The three fossil sites are geographically very close to each other, suggesting that they have probably
145 witnessed similar climatic histories during the Holocene.

146 Pollen-based numerical calibration models for both PANN and TANN were established using the
147 Chinese surface pollen–climate database which has been shown to be robust and reliable for Holocene
148 climatic inferences that have been described elsewhere in more detail (e.g. Zheng et al. 2008, 2014; Li
149 et al. 2014, 2015, 2017). The technique in terms of weighted averaging-partial least squares (WA-PLS;
150 ter Braak and Juggins 1993) regression and calibration was chosen for constructing the pollen-based
151 reconstruction models for PANN as well as TANN, because it has been successfully employed in a
152 large number of empirical, theoretical and practical studies; and has been shown to perform as well as
153 or better in comparison with other statistical regression approaches that are commonly applied for
154 developing pollen-based calibration models for regional, continental and global scales (e.g. Birks 1998;
155 Seppä et al. 2009; Birks et al. 2010; Salonen et al. 2012; Li et al. 2015, 2017). The performance of all
156 WA-PLS models was assessed with the method of leave-one-out cross-validation (Birks 1998). The
157 calculated model statistics for PANN and TANN embrace coefficient of determination (R^2) between
158 measured and predicted data, root-mean-square-error of prediction (RMSEP), and maximum bias. The
159 two-component WA-PLS models (Fig. 2) were selected with respect to high R^2 , low RMSEP and
160 maximum bias, as well as the smallest number of useful components (Birks 1998). All terrestrial pollen
161 taxa were taken into account and their percentage values were square-root transformed to reduce noises
162 and stabilize variances in the pollen data (Prentice 1980). The constructions or evaluations of all WA-

163 PLS models associated with the numerical PANN or TANN estimates were carried out using the C2
164 software (Juggins 2007). In addition, it has been demonstrated elsewhere that PANN and TANN are
165 not always strongly correlated and that either PANN or TANN is statistically significant as well as
166 ecologically meaningful in influencing broad-scale pollen distribution, indicating that they can be
167 employed simultaneously for the pollen-based palaeoclimatic reconstructions applied here (e.g. Li et
168 al. 2014, 2015).

169 To obtain the underlying characteristics and summarize the potential regional signals, a total of six
170 quantitative climatic reconstructions based on the three fossil pollen datasets were integrated to
171 produce two general high-resolution Holocene climatic sequences (PANN and TANN) for the lower
172 Yangtze region of China. Such a composite methodology has been successfully used for quantitative
173 pollen-derived and regional-scale Holocene climatic reconstructions in Europe (e.g. Seppä et al. 2009;
174 Salonen et al. 2014; Mauri et al. 2015), North America (e.g. Viau et al. 2006, 2012; Ladd et al. 2015),
175 and northern China (e.g. Li et al. 2015, 2017). It can be described briefly as follows. Each PANN or
176 TANN estimate was calculated as deviations from their mean values across the Holocene. All
177 estimated values of individual reconstructions for PANN or TANN were then combined so as to
178 prepare two Holocene climatic records with an average time-resolution of circa 36 years for both
179 PANN and TANN. Power spectra for potential periodicities in the pollen-stacked precipitation and
180 temperature records were performed using the Redfit software (Schulz and Mudelsee 2002). This
181 software is able to deal with unevenly distributed time-series data, and can test statistical significance
182 of the spectral peaks against the red-noise background with a null-hypothesis, which can be evaluated
183 by utilizing the first-order autoregressive signals, where characteristic time-scales as well as sampled
184 time-spans match those of the real data, without the necessity for any interpolation (Schulz and
185 Mudelsee 2002).

186 **4 Results and discussion**

187 **4.1 Climatic reconstructions with low- and high-frequency trends**

188 The pollen-inferred site-specific Holocene climatic reconstructions are presented in Figure 3. The
189 regionally-averaged estimates are shown in Figure 4. Thus we provide the first ~36-year resolution

190 pairwise-dataset for both PANN and TANN records covering the last 10,000 years. These portray both
191 general patterns as well as detailed features of the Holocene rainfall and temperature variations for the
192 lower reaches of the Yangtze catchment. Power spectrum analyses conducted for the composite
193 reconstructions reveal significant periodicities of 4000, 1190, and 116 years for PANN, and of 2500,
194 1190, and 116 years for TANN (Fig. 5). Some of these periodicities can also be found in other Holocene
195 Asian monsoonal records and various solar parameters (e.g. Li et al. 1996; Laskar et al. 2004; Dykoski
196 et al. 2005; Wang et al. 2008; Wanner et al. 2008, 2011; Zhao and Feng 2014), suggesting a possible
197 mechanistic connection among these climatic systems.

198 Overall high-frequency PANN and TANN fluctuations concurrently show a maximum level between
199 10,000 and 7000 cal. yr BP, and a generally declining pattern with strong oscillations from 7000 cal.
200 yr BP to the present-day (Fig. 4). The early to middle Holocene had high values of PANN and TANN,
201 suggesting a warm, wet climate and a strong East Asian summer monsoon, as also demonstrated by
202 rapidly increased sea level and possible small paddy rice cultivation in the LYR coastal plain (e.g.
203 Innes et al. 2009; Shu et al. 2010; Zong et al. 2011; Wang et al. 2012). Subtropical forests were regarded
204 as the dominant regional biome during this time phase, with *Castanopsis* and *Cyclobalanopsis*
205 identified as the major tree taxa, which is evident in many published fossil pollen records from different
206 parts of the LYR region (e.g. Chen et al. 2005; Yi et al. 2006; Innes et al. 2009; Wu et al. 2010; Li et
207 al. 2012). However, since approximately 7000~5000 cal. yr BP, the cool temperate forest elements
208 such as *Quercus*, *Betula* and *Alnus* started to occur and expanded while subtropical elements decreased,
209 eventually leading to a mixed temperate–evergreen vegetation type which prevailed until modern times.
210 The relative sea level was stable with only small fluctuations observed for this time period (e.g. Huang
211 and Zhang 2000; Shu et al. 2007; Yi et al. 2006; Innes et al. 2014). This is closely in line with our
212 climatic reconstructions displaying a falling trend for PANN and TANN values during this period,
213 implying a cooling and drying climate associated with a gradually weakening EASM intensity from
214 the middle to late Holocene in the LYR area (Fig. 4). In addition, it is noteworthy that in eastern
215 monsoonal China, human activity played an important role in influencing vegetation cover during the
216 late Holocene especially the last 2000 years (e.g. Zhao et al. 2009), which implies that pollen-based
217 climatic inferences should thus be treated with caution (e.g. Li et al. 2014).

218 Several low-frequency cooling and drying episodes can be clearly detected from our pollen-
219 estimated PANN and TANN records. These cold and dry climatic events at about 5300, 4200, 2800
220 cal. yr BP and during the Little Ice Age interval in the LYR region (Fig. 4) appear to be correlated well
221 with those widely reported from other areas in China (e.g. Wang et al. 2005; Shao et al. 2006; Xu et
222 al. 2010; Innes et al. 2014), the North Atlantic region (e.g. Bond et al. 2001; Seppä et al. 2009), and
223 the Northern Hemisphere (e.g. Clemens 2005; Vialou et al. 2006; Wanner et al. 2008, 2011). Such short-
224 lived climatic events with high amplitude have been suggested to play a significant role in driving the
225 demise and termination of Neolithic civilization such as the Liangzhu Culture in the Yangtze lowland
226 area, because prehistorical farming fields and human settlements were usually situated close to water
227 bodies such as lake shores and river channels, leading to these agricultural lands and cultural systems
228 becoming vulnerable to abrupt changes in water supplies and thermal conditions during the Holocene,
229 for example during the Neoglacial epoch (e.g. Zhang et al. 2005; Yao et al. 2008; Huang et al. 2010;
230 Wu et al. 2010; Innes et al. 2014).

231 **4.2 Comparison with other subtropical or tropical Holocene records and possible mechanisms**

232 A decadal- to centennial-scale comparison of our pollen-based PANN and TANN estimates for the
233 LYR with other related Holocene climatic proxy records from subtropical China, the Indian summer
234 monsoon (ISM)-influenced region and other tropical or subtropical regions of the world, indicates a
235 macro-scale in-phase pattern of general variability, exhibiting a consistent early Holocene climatic
236 optimum in precipitation or temperature but a relatively dryer or cooler middle to late Holocene (Fig.
237 6). However, it is notable that this general pattern is different to that indicated by two Holocene
238 hydrological records from the middle reaches of the Yangtze River, that is, the mass accumulation rates
239 of hopanoids from Dajiuhu peat bog as a proxy for water level, and the ratio of anhysteretic remanent
240 magnetization (ARM) to saturation isothermal remanent magnetization (SIRM) from a stalagmite in
241 Heshang Cave as a magnetic proxy, both suggesting a dry middle Holocene but a wetter early or late
242 Holocene (Xie et al. 2013). These two records are also inconsistent with other proxy-based climatic
243 records from the same region, for example, the pollen-based TANN record from Dajiuhu peat (Zhu et
244 al. 2008) and the stalagmite $\delta^{18}\text{O}$ record from Heshang Cave (Hu et al. 2008), which are in good
245 agreement with our Holocene PANN and TANN records for the LYR. This discrepancy may result

246 from the differences in the various reconstruction techniques, distinct temporal resolutions, reliability
247 of sedimentary chronologies, climatic significance of diverse proxy indicators, or spatial
248 representativeness of sampled sites (e.g. Liu et al. 2015; Rao et al. 2016; Chen et al. 2016a). In addition,
249 the aforementioned Holocene climatic records with consistent patterns that cover a broad geographical
250 region include the following proxy datasets: the mean summer solar insolation (Laskar et al. 2004);
251 stalagmite $\delta^{18}\text{O}$ records from Dongge (Dykoski et al. 2005), Sanbao (Wang et al. 2008) and Qunf
252 (Fleitmann et al. 2003) Caves; a model-simulated PANN record for southwestern China (Chen et al.
253 2014); a pollen-inferred PANN estimate for Xingyun Lake in the ISM-influenced Yunan Province
254 (Chen et al. 2014); a TANN reconstruction from Dajiuhu wetland in the EASM-dominated Hubei
255 Province (Zhu et al. 2008); pollen-estimated moisture index (Zhao et al. 2009) as well as tree cover
256 reconstruction (Tian et al. 2016) for southern China; a humification record from Hongyuan wetland on
257 the southeastern Tibetan Plateau (Yu et al. 2006); a synthesized moisture index based on various proxy
258 data for the southern Tibetan Plateau (Ran and Feng 2013); total organic carbon (Yancheva et al. 2007)
259 and tree pollen records (Wang et al. 2007) from Huguangyan Maar Lake in southern China; an ISM
260 rainfall index based on 92 monsoonal moisture records in eastern Asia (Wang et al. 2010); the
261 Intertropical Convergence Zone (ITCZ) index inferred from Ti contents in Cariaco Basin, Venezuela
262 (Haug et al. 2001); a *Globigerina bulloides* record from a marine sediment core in Arabian Sea (Gupta
263 et al. 2005); composite sea surface temperature (SST) records for Western Pacific Warm Pool (WPWP;
264 Scott et al. 2004; Koutavas and Joanides 2012); and an El Niño/Southern Oscillation (ENSO) record
265 from Laguna Pallcacocha, Ecuador (Moy et al. 2002). Of these records, it is worth noting that the
266 Holocene stalagmite $\delta^{18}\text{O}$ data have been lately argued to probably represent a signal of the isotopic
267 composition of precipitation from the ISM-influenced region rather than the EASM-dominated
268 territory (e.g. Chen et al. 2014; Yang et al. 2014; Wang et al. 2014; Liu et al. 2015; Chen et al. 2016a).

269 The above multiple lines of evidence suggest a strong causal linkage between tropical and
270 subtropical climatic systems from the perspective of hemispheric or global scale teleconnections (Fig.
271 6). It has been often proposed in earlier studies that the orbitally-controlled variability of summer solar
272 insolation would have essentially modulated and triggered the tropical and subtropical summer
273 monsoonal evolution during the post-glacial Holocene epoch (e.g. An et al. 2000; Gupta et al. 2005;

274 Fleitmann et al. 2003; Wang et al. 2008; Zhao et al. 2009; Koutavas and Tsukamoto 2014). During the
275 early Holocene, the high output of summer insolation may have caused the northward migration of
276 both mean ITCZ and Western Pacific Subtropical High (WPSH) positions as indicated clearly by the
277 high SST values in the WPWP and the Arabian Sea. This therefore resulted in a great amount of
278 evaporated water vapor being transported from the tropical and subtropical oceanic areas to southern
279 and eastern Asia, leading to the northward expansion and penetration of the overall summer monsoonal
280 strength as well as its extensive rain band, and thus abundant rainfall as well as high temperature in
281 the low-latitude regions of monsoonal Asia (e.g. Scott et al. 2004; Zhao et al. 2007; Zhou et al. 2009;
282 Sun and Feng 2013). In contrast, during the middle to late Holocene, a reduced summer insolation
283 would have brought about the southward retreat of both ITCZ and WPSH zones along with the
284 decreased pattern of tropical SST values, which led to a lower moisture transportation from the ocean
285 to continental lands, thereby causing the southward shift and weakening of the summer monsoonal
286 intensity and its rain belt, and reduced rainfall as well as lower heat content in the southern part of
287 monsoonal Asia and China (e.g. Dykoski et al. 2005; Wang et al. 2008; Sun and Feng 2013). In addition,
288 an overall stepwise intensification of ENSO activity from the early to late Holocene (Fig. 6) has been
289 suggested to bring warm water masses with higher SST to the eastern Tropical Pacific Ocean, resulting
290 in lower SST in the western Tropical Pacific Ocean, thus progressively reducing the transport of water
291 vapor to monsoonal China during the entire Holocene (e.g. Wang et al. 2000; Higginson et al. 2004;
292 Sun and Feng 2013).

293 **4.3 Comparison with Holocene climatic records from northern monsoonal and the westerlies'** 294 **region of China**

295 A detailed comparison of our inferred precipitation and temperature reconstructions for the LYR with
296 other high-resolution Holocene moisture and temperature records in the monsoonal regions of northern
297 China and in the westerly-dominated areas of northwestern China, reveal an out-of-phase pattern of
298 overall climatic shifts and a major offset in relation to timings of the Holocene climatic optimum
299 interval (Fig. 7). These early published records consist of the following datasets: pollen-reconstructed
300 annual rainfall series from Gonghai Lake (Chen et al. 2015) on the Chinese Loess Plateau (CLP) and
301 Daihai Lake (Xu et al. 2010) in central Inner Mongolia; a multi-proxy based temperature

302 reconstruction for northern China (Hou and Fang 2011); an EASM index based on various proxies in
303 the northern part of monsoonal China (Wang et al. 2010); tree pollen percentages from Qinghai Lake
304 (Shen et al. 2005) and Bayanchagan Lake (Jiang et al. 2006) in northern monsoonal China; a pollen-
305 based moisture record for the northern EASM marginal region (Wang and Feng 2013); frequencies of
306 palaeosol occurrences in the CLP (Wang et al. 2014) and northern China (Li et al. 2014); frequency in
307 the formation of loess or aeolian sands in northern China (Li et al. 2014); a magnetic susceptibility
308 record from the Yulin loess–palaeosol section on the northern CLP (Lu et al. 2013); and a moisture
309 index synthesized from different proxy records for the westerly-influenced regions of Arid Central
310 Asia (ACA) including northwestern China (Chen et al. 2008).

311 The multiple Holocene climatic records, spanning a large geographical area in both northern and
312 northwestern China, point to an overwhelming signal with respect to a middle Holocene climatic
313 optimum that is characterized by the highest precipitation amounts or the warmest temperature
314 conditions (Fig. 7). Recently, Chen et al. (2016b) indicated that in the Xinjiang region as a core area
315 of ACA, magnetic susceptibility records from four loess–palaeosol profiles have exhibited an
316 increasing moisture pattern from the early to late Holocene. However, these trends are out-of-phase
317 with a typical signal of an early Holocene climatic optimum demonstrated by our pollen-stacked PANN
318 or TANN reconstructions for the LYR region as well as other Holocene monsoonal records from the
319 subtropical and tropical domains of China or the ISM-dominated regions presented in this study (Fig.
320 6). Such an inconsistency may have arisen from unreliable dating controls, various proxy
321 interpretations and resolutions, or different methodological issues and assumptions (e.g. Zhao et al.
322 2009; Cai et al. 2010; Sun and Feng 2013; Liu et al. 2015). In addition, the climatological viewpoints
323 with regard to this notable timing mismatch remain under debate, which can be tentatively attributed
324 to the significant cooling effect at a hemispherical-scale caused by the deglaciation of broad-scale
325 remnant ice sheets in the high-latitude territories of the Northern Hemisphere during the early
326 Holocene (Fig. 7) (e.g. Chen et al. 2008; Renssen et al. 2012; Li et al. 2015; Liu et al. 2015; Mjell et
327 al. 2015). The rapid melting of these remnant ice sheets such as the Laurentide Ice Sheet (Jennings et
328 al. 2015) in North America and the Agassiz Ice Cap (Fisher et al. 2012) in Greenland, would have
329 likely yielded a large body of freshwater discharge into the northern Atlantic Ocean (Fig. 7). This may

330 have resulted in a suppressed Atlantic meridional overturning circulation (AMOC) as well as North
331 Atlantic Deep Water circulation (NADW), and at the same time increased Ice-Rafted Debris (IRD) in
332 ocean sediments, massive glacial advances, strong meridional temperature gradient and westerly
333 airstreams, and intensified Siberian High and winter monsoon strength, which may in turn have played
334 an important role in blocking the northward movements of the summer monsoon as well as its rainfall
335 front to the northern part of monsoonal China during the early Holocene (Fig. 7) (e.g. Zhao et al. 2009;
336 Chen et al. 2015; Li et al. 2015; Liu et al. 2015).

337 **Conclusions**

338 Here we present a pollen-based Holocene climatic dataset with a ~36-year resolution for both PANN
339 and TANN records over the last 10,000 years for the lower reaches of the Yangtze basin in eastern
340 monsoonal China. Our reconstructions show that precipitation and temperature have a concurrent trend
341 of variability on a centennial- to multidecadal timescale, implying a notable climatic pattern of moist-
342 warm or dry-cool intervals during the Holocene. Multi-proxy comparisons indicate that regional-scale
343 Holocene rainfall and thermal variations in the lower Yangtze area are in good agreement with other
344 Holocene climatic records from southern monsoonal China or the ISM-dominated regions, suggesting
345 an early Holocene climatic optimum that was characterized by high precipitation and warm conditions,
346 and a drying or cooling climate for the middle to late Holocene. The orbitally-triggered changes of
347 summer solar insolation and tropical or subtropical climatic circulations such as ITCZ, WPSH, and
348 ENSO may be recognized as the important driving factors for the Holocene summer monsoon
349 variability in the lower Yangtze region of China. Further regional inter-comparisons reveal that the
350 LYR Holocene climatic development has been different to the Holocene moisture or thermal records
351 from the EASM-influenced northern China and the westerly-affected northwestern China where the
352 Holocene climatic optimum mostly took place during the middle Holocene. Overall, our pollen-based
353 high-resolution climatic dataset may be useful for validating climate model simulations, understanding
354 the nature of monsoon climate, and predicting future climatic scenarios in monsoonal Asia and its
355 surrounding areas. Clearly, more case studies would enhance understanding the nature of Holocene
356 climatic changes in different bioclimatic regions of monsoonal China.

357 **Acknowledgments**

358 This work was financially funded by projects from the State Key Laboratory of Loess and Quaternary
359 Geology in the Institute of Earth Environment of the Chinese Academy of Sciences (Y652001589 and
360 Y651031589), the West Light Foundation of The Chinese Academy of Sciences (XAB2016B01), the
361 National Science Foundation of China (NSFC 41522305 and 41403018), the Major State Basic
362 Research Development Program (973 Program) of China (2013CB955900), and other projects from
363 the Chinese Academy of Sciences (QYZDB-SSW-DQC001, 132B61KYSB20160003, and
364 55ZZBS1304101).

365 **References**

366 An ZS (2000) The history and variability of the East Asian paleomonsoon climate. *Quat Sci Rev*
367 19:171–187

368 Atahan P et al. (2008) Holocene-aged sedimentary records of environmental changes and early
369 agriculture in the lower Yangtze, China. *Quat Sci Rev* 27:556–570

370 Bartlein PJ et al (2011) Pollen-based continental climate reconstructions at 6 and 21 ka: a global
371 synthesis. *Clim Dyn* 37:775–802

372 Birks HJB (1998) Numerical tools in palaeolimnology: progress, potentialities, and problems. *J*
373 *Paleolimnol* 20:307–332

374 Birks HJB, Heiri O, Seppä H, Bjune AE (2010) Strengths and weaknesses of quantitative climate
375 reconstructions based on late-Quaternary biological proxies. *Open Ecol J* 3:68–110

376 Bond G, Kromer B, Beer J, Muscheler R, Evans MN, Showers W, Hoffmann S, Lotti-Bond R, Hajdas
377 I, Bonani G (2001) Persistent solar influence on North Atlantic climate during the Holocene.
378 *Science* 278:1257–1266

379 Braconnot P, Harrison S, Kageyama M, Bartlein J, Masson V, Abe-Ouchi A, Otto-Bliesner B, Zhao Y
380 (2012) Evaluation of climate models using palaeoclimatic data. *Nat Clim Change* 2:417–424

381 Cai YJ, Tan LC, Cheng H, An ZS, Edwards RL, Kelly MJ, Kong XG, Wang XF (2010) The variation
382 of summer monsoon precipitation in central China since the last deglaciation. *Earth Planet Sci*
383 *Lett* 291:21–31

384 Chen FH et al (2008) Holocene moisture evolution in arid central Asia and its out-of-phase relationship
385 with Asian monsoon history. *Quat Sci Rev* 27:351–364

386 Chen FH et al (2015) East Asian summer monsoon precipitation variability since the last deglaciation.
387 *Sci Rep* 5:11186

388 Chen FH, Chen XM, Chen JH, Zhou AF, Wu D, Tang LY, Zhang XJ, Huang XZ, Yu JQ (2014)
389 Holocene vegetation history, precipitation change and Indian summer monsoon evolution
390 documented by Xingyun Lake, Southwest China. *J Quat Sci* 29:661–674

391 Chen FH, Jia J, Chen JH, Li GQ, Zhang XJ, Xie HC, Xia DS, Huang W, An CB (2016b) A persistent
392 Holocene wetting trend in arid central Asia, with wettest conditions in the late Holocene, revealed
393 by multi-proxy analyses of loess-paleosol sequences in Xinjiang, China. *Quat Sci Rev* 146:134–
394 146

395 Chen FH, Wu D, Chen JH, Zhou AF, Yu JQ, Shen J, Wang SM, Huang XZ (2016a) Holocene moisture
396 and East Asian summer monsoon evolution in the northeastern Tibetan Plateau recorded by Lake
397 Qinghai and its environs: A review of conflicting proxies. *Quat Sci Rev* 154:111–129

398 Chen W, Wang W, Dai X (2009) Holocene vegetation history with implications of human impact in
399 the Lake Chaohu area, Anhui Province, East China. *Veget Hist Archaeobot* 18:137–146

400 Chen Z, Wang Z, Schneiderman J, Tao J, Cai Y (2005) Holocene climate fluctuations in the Yangtze
401 delta of eastern China and the Neolithic response. *Holocene* 15:915–924

402 Clemens SC (2005) Millennial-band climate spectrum resolved and linked to centennial-scale solar
403 cycles. *Quat Sci Rev* 24:521–531

404 Dyke AS (2004) An outline of North American deglaciation with emphasis on central and northern
405 Canada. *Dev Quat Sci* 2:373–424

406 Dykoski CA, Edwards RL, Cheng H, Yuan DX, Cai YJ, Zhang ML, Lin YS, Qing JM, An ZS,
407 Revenaugh J (2005) A high-resolution, absolute-dated Holocene and deglacial Asian monsoon
408 record from Dongge Cave, China. *Earth Planet Sci Lett* 233:71–86

409 Fisher D, Zheng J, Burgess D, Zdanowicz C, Kinnard C, Sharp M, Bourgeois J (2012) Recent melt
410 rates of Canadian arctic ice caps are the highest in four millennia. *Glob Planet Change* 84–85:3–
411 7

412 Fleitmann D, Burns SJ, Mudelsee M, Neff U, Kramers J, Mangini A, Matter A (2003) Holocene forcing
413 of the Indian monsoon recorded in a stalagmite from southern Oman. *Science* 300:1737–1739

414 Fuller DQ, Qin L, Zheng Y, Zhao Z, Chen X, Hosoya LA, Sun GP (2009) The domestication process
415 and domestication rate in rice: spikelet bases from the lower Yangtze. *Science* 323:1607–1610

416 Gupta AK, Das M, Anderson DM (2005) Solar influence on the Indian summer monsoon during the
417 Holocene. *Geophys Res Lett* 32:L17703

418 Haug GH, Hughen KA, Sigman DM, Peterson LC, Röhl U (2001) Southward migration of the
419 Intertropical Convergence Zone through the Holocene. *Science* 293:1304–1308

420 Heiri O et al (2014) Validation of climate model-inferred regional temperature change for late-glacial
421 Europe. *Nat Commun* 5:4914

422 Herzschuh U, Kramer A, Mischke S, Zhang CJ (2009) Quantitative climate and vegetation trends since
423 the late glacial on the northeastern Tibetan Plateau deduced from Koucha Lake pollen spectra.
424 *Quat Res* 71:162–171

425 Higginson MJ, Altabet MA, Lauren W, Herbert TD, Murray DW (2004) A solar (irradiance) trigger
426 for millennial-scale abrupt changes in the southwest monsoon? *Paleoceanography* 19:77–100

427 Hou GL, Fang X (2011) Characteristics analysis and synthetical reconstruction of regional temperature
428 series of the Holocene in China. *J Palaeogeogr* 14:243–252 (in Chinese)

429 Hu CY, Henderson GM, Huang JH, Xie SC, Sun Y, Johnson KR (2008) Quantification of Holocene
430 Asian monsoon rainfall from spatially separated cave records. *Earth Planet Sci Lett* 266:221–232

431 Huang CC, Pang J, Zha XC, Zhou Y, Su H, Li Y (2010) Extraordinary floods of 4100–4000 a BP
432 recorded at the Late Neolithic ruins in the Jinghe River Gorges, middle reach of the Yellow River,
433 China. *Palaeogeogr Palaeoclimatol Palaeoecol* 289:1–9

434 Huang F, Zhang M (2000) Pollen and phytolith evidence for rice cultivation during the Neolithic at
435 Longqiuzhuang, eastern Jianghuai, China. *Veget Hist Archaeobot* 9:161–168

436 Innes JB, Zong Y, Chen Z, Chen C, Wang Z, Wang H (2009) Environmental history, palaeoecology
437 and human activity at the early Neolithic forager/cultivator site at Kuahuqiao, Hangzhou, eastern
438 China. *Quat Sci Rev* 28:2277–2294

439 Innes JB, Zong Y, Wang Z, Chen Z (2014) Climatic and palaeoecological changes during the mid- to

440 late Holocene transition in eastern china: high-resolution pollen and non-pollen palynomorph
441 analysis at Pingwang, Yangtze coastal lowlands. *Quat Sci Rev* 99:164–175

442 Jennings A, Andrews J, Pearce C, Wilson L, Olfasdottir S (2015) Detrital carbonate peaks on the
443 Labrador shelf, a 13–7 ka template for freshwater forcing from the Hudson Strait outlet of the
444 Laurentide Ice Sheet into the subpolar gyre. *Quat Sci Rev* 107:62–80

445 Jiang W, Guo Z, Sun X, Wu H, Chu G, Yuan B, Hatté C, Guiot J (2006) Reconstruction of climate and
446 vegetation changes of Lake Bayanchagan (Inner Mongolia): Holocene variability of the East
447 Asian monsoon. *Quat Res* 65:411–420

448 Jin LY, Schneider B, Park W, Latif M, Khon V, Zhang XJ (2013) The spatial–temporal patterns of
449 Asian summer monsoon precipitation in response to Holocene insolation change: a model-data
450 synthesis. *Quat Sci Rev* 85:47–62

451 Juggins S (2007) C2 Version 1.5 User guide. Software for ecological and palaeoecological data
452 analysis and visualisation. Newcastle University, Newcastle upon Tyne

453 Kalnay E, Kanamitsu M, Kistler R, Collins W, Deaven D, Gandin L, Iredell M, Saha S, White G,
454 Woollen J, Zhu Y, Leetmaa A, Reynolds R (1996) The NCEP/NCAR 40-year reanalysis project.
455 *Bull Am Meteorol Soc* 77:437–472

456 Komatsu T, Tsukamoto S (2014) Late Glacial lake-level changes in the Lake Karakul basin (a closed
457 glacierized-basin), eastern Pamirs, Tajikistan. *Quat Res* 83:137–149

458 Koutavas A, Joanides S (2012) El Niño-Southern Oscillation extrema in the Holocene and Last Glacial
459 Maximum. *Paleoceanography* 27:PA4208

460 Ladd M, Way RG, Viau AE (2015) The impact of using different modern climate data sets in pollen-
461 based paleoclimate reconstructions of north America. *Quat Sci Rev* 112:78–85

462 Laskar J, Robutel P, Joutel F, Gastineau M, Correia ACM, Levrard B, (2004) A long term numerical
463 solution for the insolation quantities of the Earth. *Astron Astrophys* 428:261–285

464 Li C, Zheng Y, Yu S, Li Y, Shen H (2012) Understanding the ecological background of rice agriculture
465 on the Ningshao plain during the Neolithic age: pollen evidence from a buried paddy field at the
466 Tianluoshan cultural site. *Quat Sci Rev* 35:131–138

467 Li JY et al (2015) East Asian summer monsoon precipitation variations in China over the last 9500

468 years: a comparison of pollen-based reconstructions and model simulations. *Holocene* 26:592–
469 602

470 Li JY et al (2017) Quantifying climatic variability in monsoonal northern China over the last 2200
471 years and its role in driving Chinese dynastic changes. *Quat Sci Rev* 159:35–46

472 Li JY, Zhao Y, Xu QH, Zheng Z, Lu HY, Luo YL, Li YC, Li CH, Seppä H (2014) Human influence as
473 a potential source of bias in pollen-based climate reconstructions. *Quat Sci Rev* 99:112–121

474 Li KJ, Su TW, Liang HF (1996) Sunspot unit areas: a new parameter describing the long-term solar
475 activity. *Chin Sci Bull* 49:2511–2516

476 Li Q, Wu H, Yu Y, Sun A, Markovic SB, Guo Z (2014) Reconstructed moisture evolution of the deserts
477 in northern China since the Last Glacial Maximum and its implications for the East Asian Summer
478 Monsoon. *Glob Planet Change* 121:101–112

479 Li Y, Wu J, Hou S, Shi C, Mo D, Liu B, Zhou L (2010) Palaeoecological records of environmental
480 change and cultural development from the Liangzhu and Qujialing archaeological sites in the
481 middle and lower reaches of the Yangtze River. *Quat Int* 227: 29–37

482 Liu JB, Chen JH, Zhang XJ, Li Y, Rao ZG, Chen FH (2015) Holocene East Asian summer monsoon
483 records in northern China and their inconsistency with Chinese stalagmite $\delta^{18}\text{O}$ records. *Earth Sci*
484 *Rev* 148:194–208

485 Londo JP, Chiang YC, Hung KH, Chiang TH, Schaal BA (2006) Phylogeography of Asian wild rice,
486 *Oryza rufipogon*, reveals multiple independent domestications of cultivated rice, *Oryza sativa*.
487 *Proc Natl Acad Sci USA* 103:9578–9583

488 Lu HY et al (2013) Variation of East Asian monsoon precipitation during the past 21 k.y. and potential
489 CO_2 forcing. *Geology* 41:1023–1026

490 Mauri A, Davis BAS, Collins PM, Kaplan JO (2015) The climate of Europe during the Holocene: a
491 gridded pollen-based reconstruction and its multi-proxy evaluation. *Quat Sci Rev* 112:109–127

492 Mjell TL, Ninnemann US, Eldevik T, Kleiven HF (2015) Holocene multidecadal- to millennial-scale
493 variations in Iceland-Scotland overflow and their relationship to climate. *Paleoceanography*
494 30:558–569

495 Morrill C, Overpeck JT, Cole JE (2003) A synthesis of abrupt changes in the Asian summer monsoon

496 since the last deglaciation. *Holocene* 13:465–476

497 Moy CM, Seltzer GO, Rodbell DT, Anderson DM (2002) Variability of El Niño/Southern Oscillation
498 activity at millennial timescales during the Holocene epoch. *Nature* 420:162–165

499 Prentice IC (1980) Multidimensional scaling as a research tool in Quaternary palynology: a review of
500 theory and methods. *Rev Palaeobot Palynol* 31:71–104

501 Ran M, Feng Z (2013) Holocene moisture variations across china and driving mechanisms: a synthesis
502 of climatic records. *Quat Int* 313:179–193

503 Rao ZG, Li YX, Zhang JW, Jia GD, Chen FH (2016) Investigating the long-term palaeoclimatic
504 controls on the δD and $\delta^{18}O$ of precipitation during the Holocene in the Indian and East Asian
505 monsoonal regions. *Earth Sci Rev* 159:292–305

506 Reimer PJ et al (2013) IntCal13 and Marine13 radiocarbon Age calibration curves 0–50,000 years cal
507 BP. *Radiocarbon* 55:1869–1887

508 Ren G, Beug HJ (2002) Mapping Holocene pollen data and vegetation of China. *Quat Sci Rev*
509 21:1395–1422

510 Renssen H, Seppä H, Crosta , Goosse H, Roche DM (2012) Global characterization of the Holocene
511 Thermal Maximum. *Quat Sci Rev* 48:7–19

512 Salonen JS, Ilvonen L, Seppä H, Holmström L, Telford RJ, Gaidamavicius A, Stancikaite M, Subetto
513 D (2012) Comparing different calibration methods (WA/WA-PLS regression and Bayesian
514 modelling) and different-sized calibration sets in pollen-based quantitative climate reconstruction.
515 *Holocene* 22:413–424

516 Salonen JS, Luoto M, Alenius T, Heikkilä M, Seppä H, Telford RJ, Birks HJB (2014) Reconstructing
517 palaeoclimatic variables from fossil pollen using boosted regression trees: comparison and
518 synthesis with other quantitative reconstruction methods. *Quat Sci Rev* 88:69–81

519 Schulz M, Mudelsee M (2002) REDFIT: estimating red-noise spectra directly from unevenly spaced
520 paleoclimatic time series. *Comput Geosci* 28:421–426

521 Seppä H, Bjune AE, Telford RJ, Birks HJB, Veski S (2009) Last nine-thousand years of temperature
522 variability in Northern Europe. *Clim Past* 5:523–535

523 Shao X, Wang Y, Cheng H, Kong X, Wu J, Edwards RL (2006) Long-term trend and abrupt events of

524 the Holocene Asian monsoon inferred from a stalagmite $d^{18}O$ record from Shennongjia in central
525 China. *Chin Sci Bull* 51:1–8

526 Shen CM, Liu KB, Morrill C, Overpeck JT, Peng JL, Tang LY (2008) Ecotone shift and major droughts
527 during the mid-late Holocene in the central Tibetan Plateau. *Ecology* 89:1079–1088

528 Shen J, Liu XQ, Wang SM, Ryo M (2005) Palaeoclimatic changes in the Qinghai Lake area during the
529 last 18,000 years. *Quat Int* 136:131–140

530 Shu JW, Wang WM, Chen W (2007) Holocene vegetation and environment changes in the NW Taihu
531 plain, Jiangsu Province, East China. *Acta Micropalaeontol Sin* 24:210–221 (in Chinese)

532 Shu JW, Wang WM, Jiang LP, Takahara H (2010) Early Neolithic vegetation history, fire regime and
533 human activity at Kuahuqiao, Lower Yangtze River, East China: new and improved insight. *Quat*
534 *Int* 227:10–21

535 Stott L, Cannariato K, Thunell R, Haug GH, Koutavas A, Lund S (2004) Decline of surface
536 temperature and salinity in the western tropical Pacific Ocean in the Holocene epoch. *Nature*
537 431:56–59

538 Sun AZ, Feng ZD (2013) Holocene climatic reconstructions from the fossil pollen record at Qigai
539 Nuur in the southern Mongolian Plateau. *Holocene* 23:1391–1402

540 Tao J, Chen MT, Xu S (2006) A Holocene environmental record from the southern Yangtze River delta,
541 eastern China. *Palaeogeogr Palaeoclimatol Palaeoecol* 230:204–229

542 ter Braak CJF, Juggins S (1993) Weighted averaging partial least squares regression (WA-PLS): an
543 improved method for reconstructing environmental variables from species assemblages.
544 *Hydrobiologia* 269:485–502

545 Tian F, Cao X, Dallmeyer A, Ni J, Zhao Y, Wang Y, Herzschuh U (2016) Quantitative woody cover
546 reconstructions from eastern continental Asia of the last 22 kyr reveal strong regional peculiarities.
547 *Quat Sci Rev* 137:33–44

548 Viau AE, Gajewski K, Sawada MC, Fines P (2006) Millennial-scale temperature variability in North
549 America during the Holocene. *J Geophys Res* 111:D09102

550 Viau AE, Ladd M, Gajewski K (2012) The climate of north America during the past 2000 years
551 reconstructed from pollen data. *Glob Planet Change* 84–85:75–83

- 552 Wang B, Wu R, Fu X (2000) Pacific–East Asia teleconnection: how does ENSO affect East Asian
553 climate? *J Clim* 13:1517–1536
- 554 Wang H, Chen J, Zhang X, Chen F (2014) Palaeosol development in the Chinese Loess Plateau as an
555 indicator of the strength of the East Asian summer monsoon: evidence for a mid-Holocene
556 maximum. *Quat Int* 334:155–164
- 557 Wang S, Lü H, Liu J, Negendank JW (2007) The early Holocene optimum inferred from a high-
558 resolution pollen record of Huguangyan Maar Lake in southern China. *Chin Sci Bull* 52:2829–
559 2836
- 560 Wang W, Feng Z (2013) Holocene moisture evolution across the Mongolian Plateau and its
561 surrounding areas: a synthesis of climatic records. *Earth Sci Rev* 122:38–57
- 562 Wang Y et al (2014) Quantitative reconstruction of precipitation changes on the NE Tibetan Plateau
563 since the Last Glacial Maximum e extending the concept of pollen source area to pollen-based
564 climate reconstructions from large lakes. *Clim Past* 10:21–39
- 565 Wang Y, Cheng H, Edwards RL, He Y, Kong X, An Z, Wu J, Kelly MJ, Dykoski CA, Li X (2005) The
566 Holocene Asian monsoon: links to solar changes and North Atlantic climate. *Science* 308:854–
567 857
- 568 Wang YB, Liu XQ, Herzschuh U (2010) Asynchronous evolution of the Indian and East Asian Summer
569 Monsoon indicated by Holocene moisture patterns in monsoonal central Asia. *Earth Sci Rev*
570 103:135–153
- 571 Wang YJ et al (2008) Millennial- and orbital-scale changes in the East Asian monsoon over the past
572 224,000 years. *Nature* 451:1090–1093
- 573 Wang Z, Li M, Zhang R, Zhuang C, Liu Y, Saito Y, Xie J, Zhao B (2011) Impacts of human activity
574 on the late-Holocene development of the subaqueous Yangtze Delta, China, as shown by magnetic
575 properties and sediment accumulation rates. *Holocene* 21:393–407
- 576 Wang Z, Zhuang C, Saito Y, Chen J, Zhan Q, Wang X (2012) Early mid-Holocene sea-level change
577 and coastal environmental response on the southern Yangtze delta plain, China: implications for
578 the rise of Neolithic culture. *Quat Sci Rev* 35:51–62
- 579 Wanner H et al (2008) Mid- to Late Holocene climate change: an overview. *Quat Sci Rev* 27:1791–

580 1828

581 Wanner H, Solomina O, Grosjean M, Ritz SP, Jetel M (2011) Structure and origin of Holocene cold
582 events. *Quat Sci Rev* 30:3109–3123

583 Wu L, Li F, Zhu C, Li B (2012) Holocene environmental change and archaeology, Yangtze River Valley,
584 China: review and prospects. *Geosci Front* 3:875–892

585 Wu L, Wang XY, Zhou KS, Mo D, Zhu C, Gao C, Zhang G, Li L, Han W (2010) Transmutations of
586 ancient settlements and environmental changes between 6000 and 2000 a BP in the Chaohu Lake
587 Basin, East China. *J Geogr Sci* 20:687–700

588 Wu W (1983) Holocene palaeogeography of the Hangzhou Bay. *Acta Geogr Sin* 38:113–126 (in
589 Chinese)

590 Xie SC et al (2013) Concordant monsoon-driven postglacial hydrological changes in peat and
591 stalagmite records and their impacts on prehistoric cultures in central China. *Geology* 41:827–
592 830

593 Xu QH, Xiao JL, Li YC, Tian F, Nakagawa T (2010) Pollen-based quantitative reconstruction of
594 Holocene climate changes in the Daihai Lake area, Inner Mongolia, China. *J Clim* 23:2856–2868

595 Yancheva G et al (2007) Influence of the intertropical convergence zone on the East Asian monsoon.
596 *Nature* 445:74–77

597 Yang XD, Wang SM, Tong GB (1996) Character of palynology and changes of monsoon climate over
598 the last 10000 years in Gucheng Lake, Jiangsu Province. *Acta Bot Sin* 38:576–581 (in Chinese)

599 Yang XL, Liu JB, Liang FY, Yuan DX, Yang Y, Lu YB, Chen FH (2014) Holocene stalagmite $\delta^{18}\text{O}$
600 records in the East Asian monsoon region and their correlation with those in the Indian monsoon
601 region. *Holocene* 24:1657–1644

602 Yao P, Huang CC, Pang JL, Zha XC, Li XG (2008) Palaeoflood hydrological studies in the middle
603 reaches of the Beiluohe River. *Acta Geogr Sin* 63:1198–1206 (in Chinese)

604 Yi S, Saito Y, Yang DY (2006) Palynological evidence for Holocene environmental change in the
605 Changjiang (Yangtze River) delta, China. *Palaeogeogr Palaeoclimatol Palaeoecol* 241:103–117

606 Yi S, Saito Y, Zhao Q, Wang P (2003) Vegetation and climate changes in the Changjiang (Yangtze
607 River) Delta, China, during the past 13,000 years inferred from pollen records. *Quat Sci Rev*

608 22:1501–1519

609 Yu XF, Zhou W, Franzen LG, Feng X, Peng C, Jull AJT (2006) High-resolution peat records for
610 Holocene monsoon history in the eastern Tibetan plateau. *Sci China Ser D Earth Sci* 49:615–621

611 Zhang Q, Zhu C, Liu CL, Jiang T (2005) Environmental change and its impacts on human settlement
612 in the Yangtze Delta, P.R. China. *Catena* 60:267–277

613 Zhao J, Chen CK (1999) *Chinese Geography* (in Chinese). Higher Education Press, Beijing

614 Zhao P, Zhu Y, Zhang R (2007) An Asian-Pacific teleconnection in summer tropospheric temperature
615 and associated Asian climate variability. *Clim Dyn* 29:293–303

616 Zhao XH, Feng XS (2014) Periodicities of solar activity and the surface temperature variation of the
617 Earth and their correlations. *Chin Sci Bull* 59:1284–1292

618 Zhao Y, Yu Z, Chen F, Zhang J, Yang B (2009) Vegetation response to Holocene climate change in
619 monsoon-influenced region of China. *Earth Sci Rev* 97:242–256

620 Zheng Z et al (2008) Comparison of climatic threshold of geographical distribution between dominant
621 plants and surface pollen in China. *Sci China Ser D Earth Sci* 51:1107–1120

622 Zheng Z et al (2014) East Asian pollen database: modern pollen distribution and its quantitative
623 relationship with vegetation and climate. *J Biogeogr* 41:1819–1832

624 Zhou X, Zhao P, Liu G (2009) Asian-Pacific Oscillation index and variation of East Asian summer
625 monsoon over the past millennium. *Chin Sci Bull* 54:3768–3771

626 Zhu C, Chen X, Zhang GS, Ma CM, Zhu Q, Li ZX, Xu WF (2008) Spore-pollen-climate factor transfer
627 function and paleoenvironment reconstruction in Dajiuhu, Shennongjia, central China. *Chin Sci*
628 *Bull* 53:42–49

629 Zong Y, Chen Z, Innes JB, Chen C, Wang Z, Wang H (2007) Fire and flood management of coastal
630 swamp enabled first rice paddy cultivation in east China. *Nature* 449:459–462

631 Zong Y, Innes JB, Wang Z, Chen Z (2011) Mid-Holocene coastal hydrology and salinity changes in
632 the east Taihu area of the lower Yangtze wetlands, China. *Quat Res* 76:69–82

633 Zong Y, Lloyd JM, Leng MJ, Yim WWS, Huang G (2006) Reconstruction of Holocene monsoon
634 history from the Pearl River estuary, southern China, using diatoms and carbon isotope ratios.
635 *Holocene* 16:251–263

636 Zong Y, Wang Z, Innes JB, Chen Z (2012) Holocene environmental change and Neolithic rice
637 agriculture in the lower Yangtze region of China: a review. *Holocene* 22:623–635

638

639 **Figure captions**

640 **Figure 1** Mean 700 hPa atmospheric airstream lines between June and August based on the
641 NCEP/NCAR Reanalysis data during the time interval of 1971–2000 (Kalnay et al. 1996). Blue plus
642 signs correspond to the localities of three fossil sites (Chaohu, Gucheng, and Pingwang) in the lower
643 reaches of the Yangtze basin. ISM, EASM, and Westerlies indicate the regions dominated by the Indian
644 and Eastern Asian summer monsoon, as well as westerly air circulation, respectively. Green dashed
645 line shows the present-day northern boundary of the Asian summer monsoon system modified from
646 Chen et al. (2008).

647 **Figure 2** Numerical performance of the calibration models for mean total annual precipitation (PANN)
648 as well as mean annual temperature (TANN) based on pollen data. Statistical parameters consist of
649 coefficient of determination (R^2) between observed and predicted values, root-mean-square-error of
650 prediction (RMSEP), and maximum (Max.) bias.

651 **Figure 3** Pollen-based quantitative reconstructions for PANN with RMSEP of 232.06 mm and TANN
652 with RMSEP of 3.62 °C at Chaohu, Gucheng and Pingwang over the last 10,000 years.

653 **Figure 4** Pollen-based PANN and TANN estimates during the last 10,000 years for the lower Yangtze
654 region of China derived from the six reconstructions in Figure 3.

655 **Figure 5** Power spectrum analyses for the pollen-stacked PANN and TANN records spanning the past
656 10,000 years.

657 **Figure 6** Holocene comparison of pollen-estimated **a** PANN and **b** TANN sequences for the lower
658 Yangtze region (LYR) of China with other related climatic records including: **c** mean summer solar
659 insolation (SI) at 65 °N (Laskar et al. 2004); stalagmite $\delta^{18}\text{O}$ series from **d** Dongge (Dykoski et al.
660 2005), **e** Sanbao (Wang et al. 2008), and **f** Qunf (Fleitmann et al. 2003) Caves; **g** Kiel Climate Model
661 (KCM)-based PANN simulation for southwestern China (Chen et al. 2014); pollen-derived **h** PANN
662 reconstruction for Xingyun Lake in Yunan Province (Chen et al. 2014) and **i** TANN reconstruction for
663 Dajiuhu wetland in Hubei Province (Zhu et al. 2008); pollen-composited **j** moisture index (MI; Zhao

664 et al. 2009) and **k** tree cover (TC; Tian et al. 2016) records for southern China (SC); **l** humification (H)
665 record from Hongyuan wetland on the southeastern Tibetan Plateau (Yu et al. 2006); **m** moisture index
666 (MI) synthesized from various proxy data from the southern Tibetan Plateau (ST; Ran and Feng 2013);
667 records of **n** total organic carbon (TOC; Yancheva et al. 2007) and **o** tree pollen percentage (TP; Wang
668 et al. 2007) from Huguangyan Maar Lake in SC; **p** Indian summer monsoon (ISM) index synthesized
669 for monsoonal China (Wang et al. 2010); **q** Intertropical Convergence Zone (ITCZ) index from
670 Venezuela (Haug et al. 2001); **r** *Globigerina bulloides* percentage record from ODP Site 723 in Arabian
671 Sea (AS; Gupta et al. 2005); **s** and **t** composite sea surface temperature (SST-1 and SST-2) records for
672 Western Pacific Warm Pool (WPWP; Scott et al. 2004; Koutavas and Joanides 2012); and **u** El
673 Niño/Southern Oscillation (ENSO) index from Ecuador (Moy et al. 2002). The grey band depicts the
674 moisture or thermal maximum during the early Holocene in southern China.

675 **Figure 7** Holocene comparison of pollen-inferred **a** PANN and **b** TANN records for the lower Yangtze
676 region (LYR) of China with other climatic proxy records from northern China and other regions of the
677 northern Hemisphere: pollen-reconstructed PANN records for **c** Gonghai Lake (Chen et al. 2015) on
678 the Chinese Loess Plateau (CLP) and **d** Daihai Lake (Xu et al. 2010) in northern China (NC); **e** multi-
679 proxy-based TANN sequence for NC (Hou and Fang 2011); **f** East Asian summer monsoon (EASM)
680 index for monsoonal China (Wang et al. 2010); tree pollen records from **g** Qinghai Lake (Shen et al.
681 2005) and **h** Bayanchagan Lake (Jiang et al. 2006) in NC; **i** pollen-based moisture index (MI) for the
682 EASM marginal region (Wang and Feng 2013); frequency distributions of palaeosol occurrences in **j**
683 CLP (Wang et al. 2014) and **k** NC (Li et al. 2014); **l** frequency formations of loess or aeolian sands
684 (AS) in NC (Li et al. 2014); **m** magnetic susceptibility (MS) record from the Yulin loess–palaeosol
685 section on CLP (Lu et al. 2013); **n** moisture index (MI) synthesized for Arid Central Asia (ACA; Chen
686 et al. 2008); melt water input (MI) from **o** the Laurentide Ice Sheet (Jennings et al. 2015) and **p** the
687 Agassiz Ice Cap (Fisher et al. 2012); **q** ice-sheet coverage in northern Hemisphere (NH; Dyke 2004);
688 and **r** Atlantic meridional overturning circulation (AMOC) index based on mean sortable silt grain size
689 (SSGS) from core GS06-144 08GC in northern Atlantic Ocean (Mjell et al. 2015). The grey band
690 shows the moisture or thermal maximum during the middle Holocene in northern monsoonal China.
691 The pink band indicates the moisture or thermal maximum during the early Holocene in southern

692 monsoonal China.

693

694 **Table 1** Summary of fossil pollen datasets for PANN and TANN reconstructions at Chaohu, Gucheng
695 and Pingwang in the lower Yangtze region of China

696

Site	Lat. (°)	Long. (°)	Elev. (m)	Num. dates	Res. (years)	Reference
Chaohu	117.39	31.56	10	10	158	Chen et al. (2009)
Gucheng	118.9	31.28	6	4	30	Yang et al. (1996)
Pingwang	120.64	30.96	1.6	5	135	Innes et al. (2014)

697 Lat. = latitude; Long. = Longitude; Elev. = Elevation; Num. = Number; Res. (yrs) = Resolution
698 (years/sample)

699

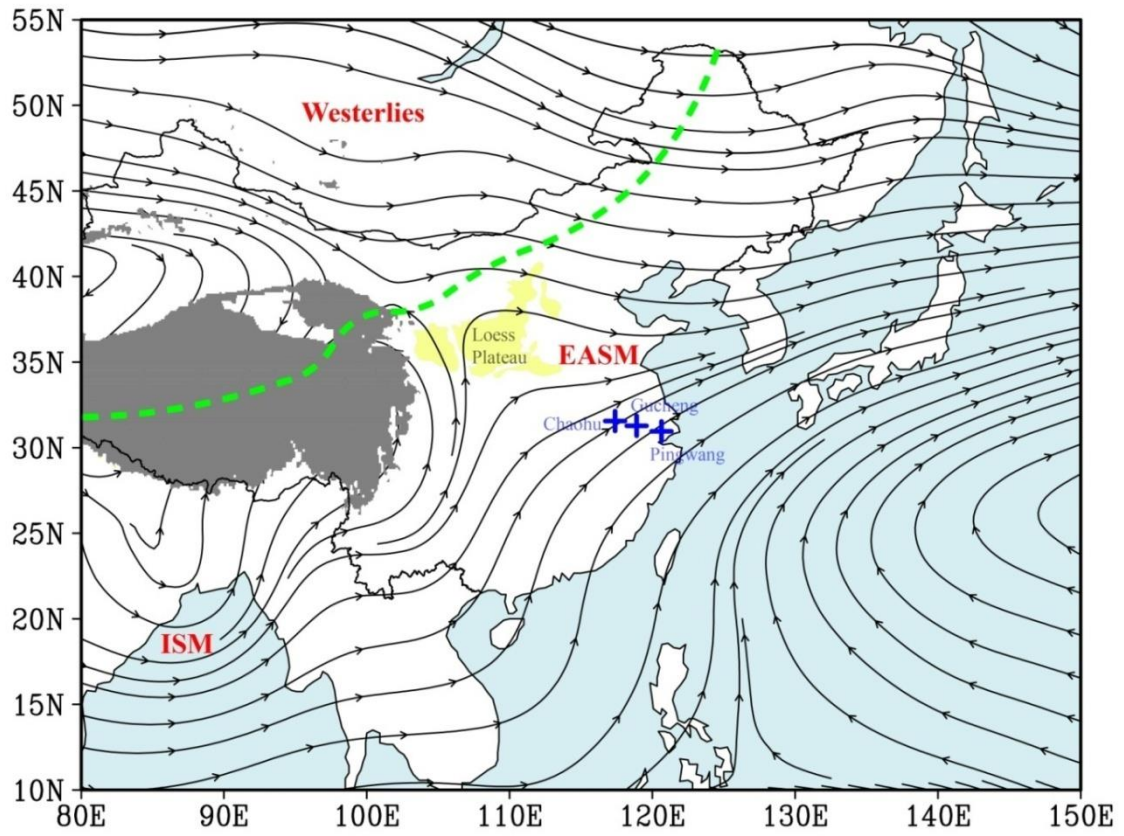
700

701

702

703

704 **Figure 1**



705

706

707

708

709

710

711

712

713

714

715

716

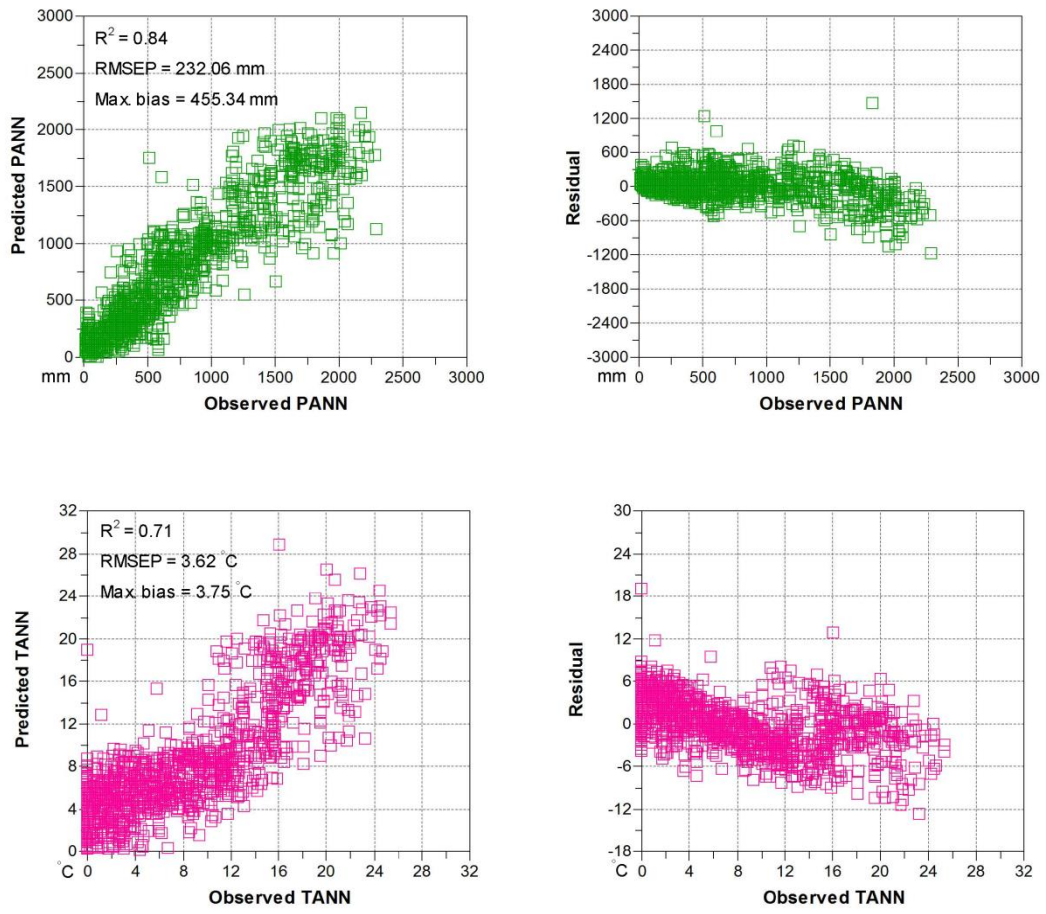
717

718

719

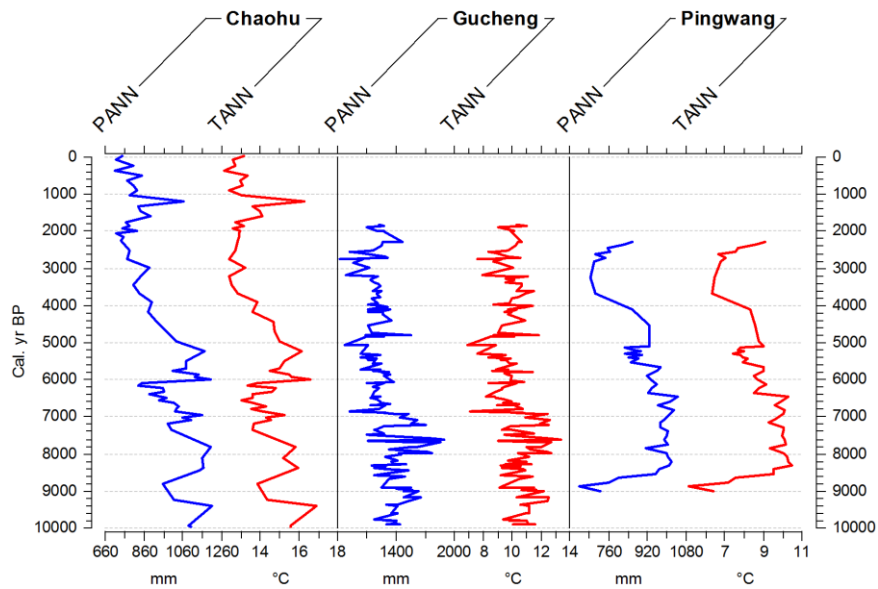
720 **Figure 2**

721



722

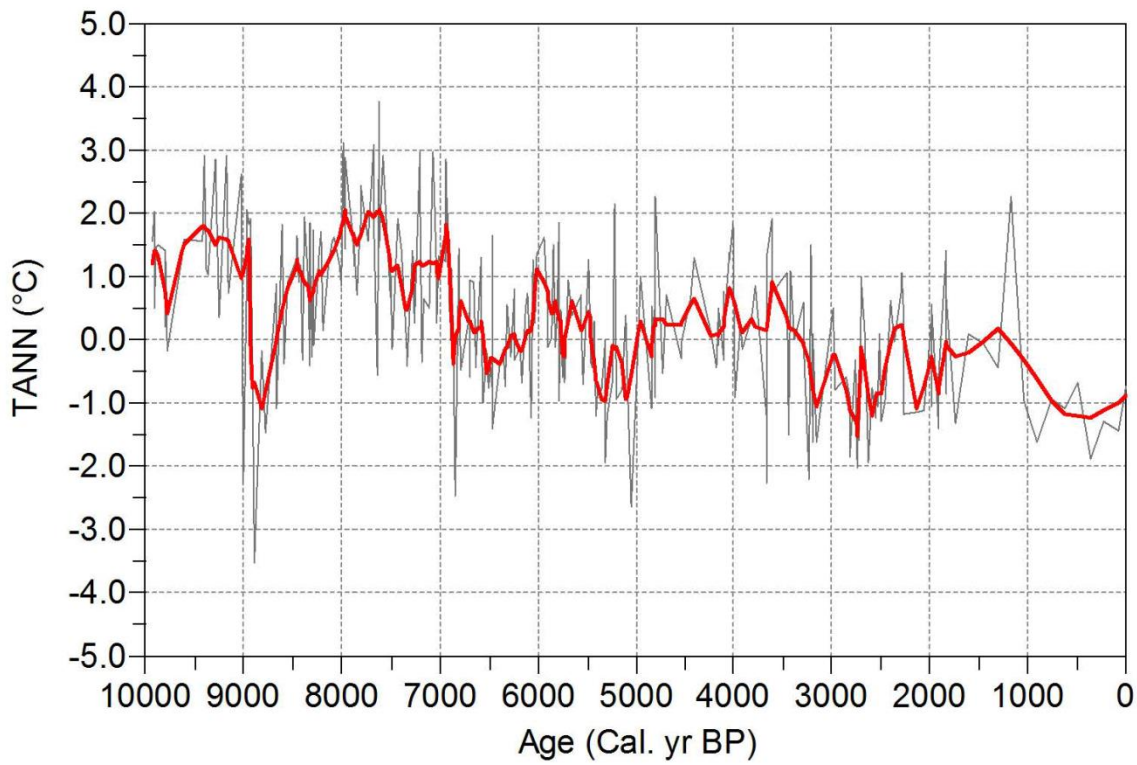
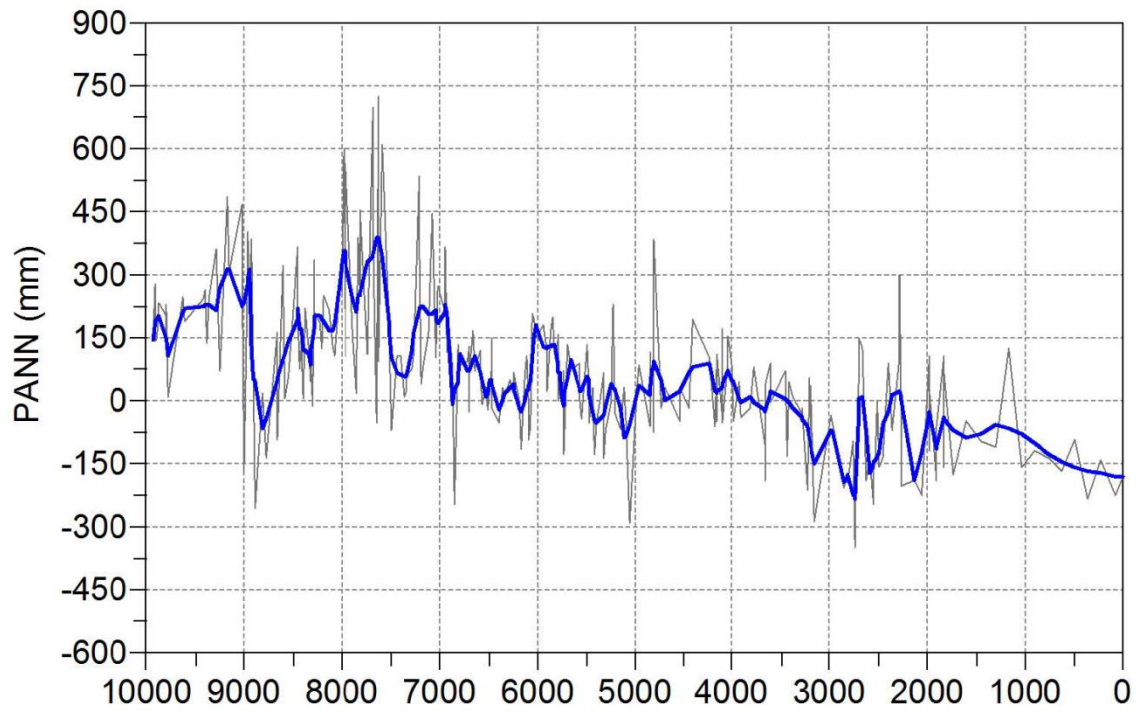
723 **Figure 3**



724

725

726 **Figure 4**



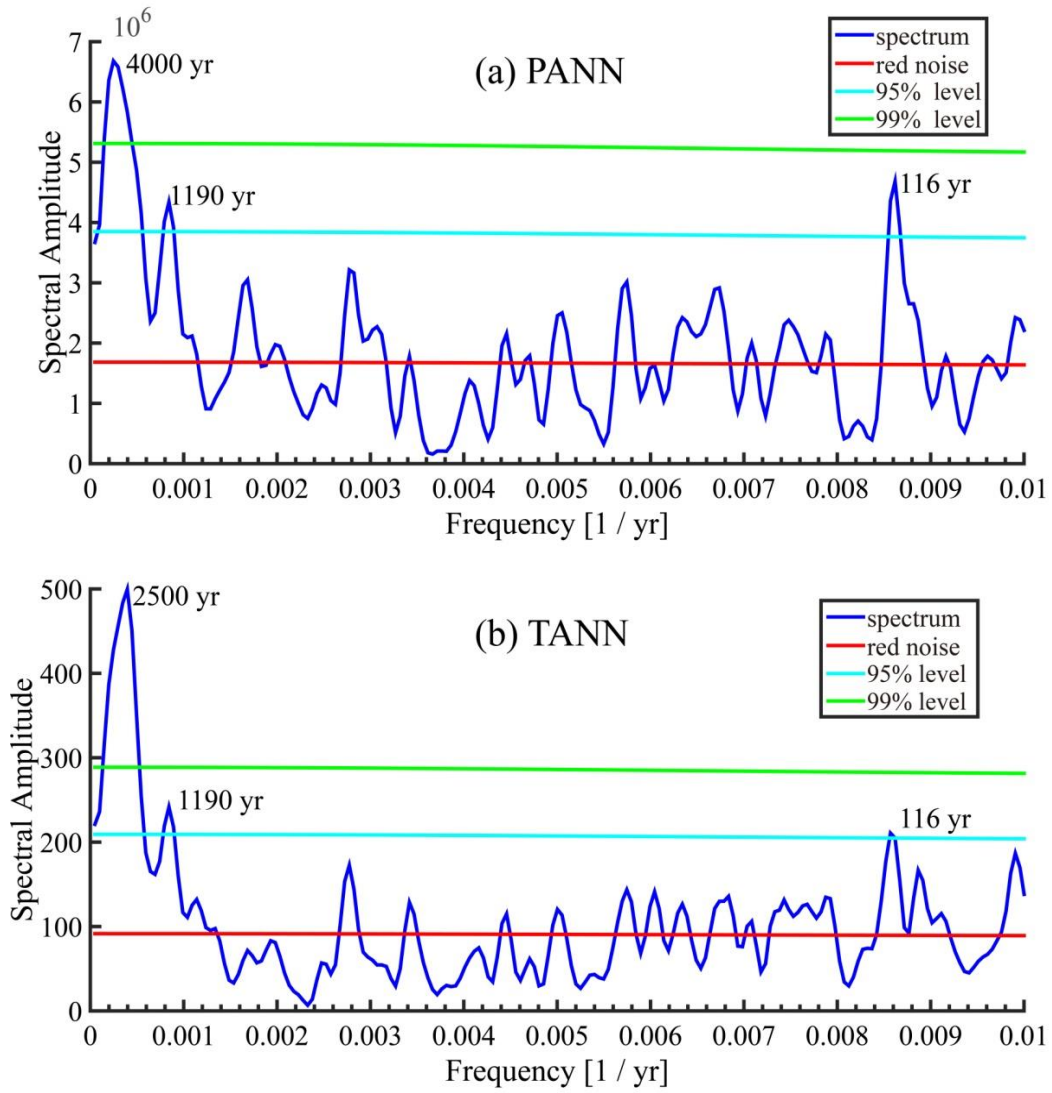
727

728

729

730 **Figure 5**

731
732
733

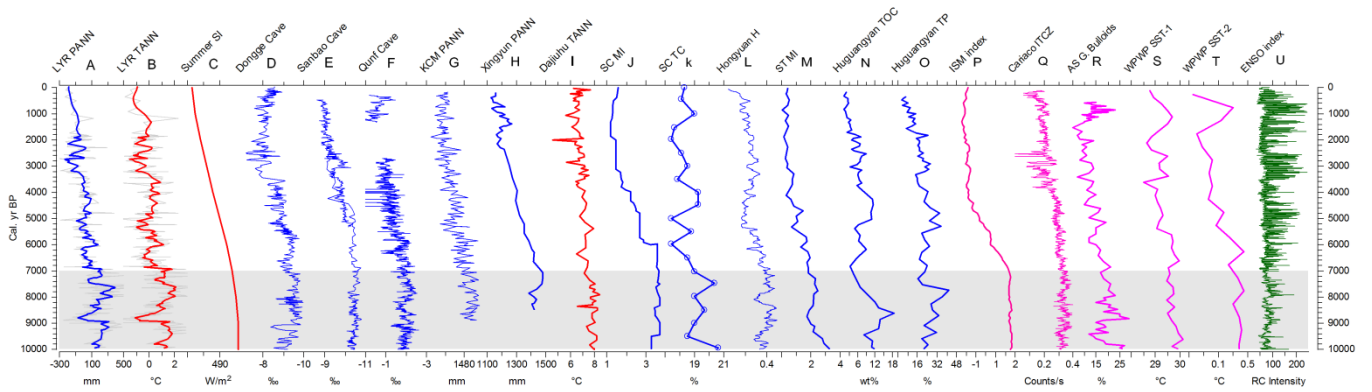


734
735
736
737
738
739
740
741
742

Figure 6

743

744



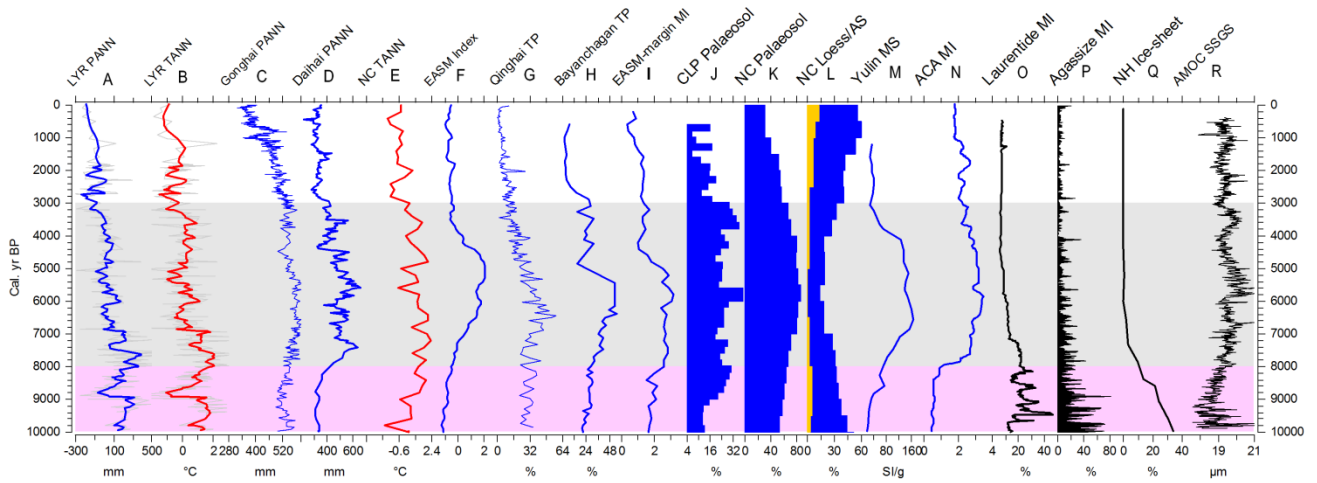
745

746

747

748

Figure 7



749